Ab initio mechanism and thermal rate constants for the reaction of atomic H with Ge_2H_6

Qingzhu Zhang, Yueshu Gu* and Shaokun Wang

School of Chemistry and Chemical Engineering, Shandong University, Jinan 250100, P. R. China. E-mail: guojz@icm.sdu.edu.cn

Received (in New Haven, CT, USA) 24th June 2002, Accepted 16th September 2002
First published as an Advance Article on the web 2nd December 2002

The reaction of digermane Ge_2H_6 with atomic H has been studied theoretically. The detailed mechanism has been revealed for the first time. This reaction involves not only abstraction but also substitution. The calculation shows that there are two transition states for the substitution reaction: (1) frontside attack of the Ge–Ge bond by the hydrogen atom and (2) backside attack of the GeH_3 group by the hydrogen atom along the Ge–Ge axis, forming a transition state structure with C_{3v} symmetry. Changes of geometries, generalized normal-mode vibrational frequencies, and potential energies along the reaction path for each channel are discussed and compared. On the basis of the *ab initio* data, the rate constants of each channel have been deduced by canonical variational transition state theory (CVT) with the small-curvature tunneling (SCT) correction method over the temperature range of 200–3000 K. The theoretical results have been compared with available experimental data. The kinetics calculations show that the variational effect is small for all the channels and in the lower temperature range, the small-curvature tunneling effect is important for the abstraction channel and the substitution channel with backside attack. At lower temperatures, the major product channel is direct hydrogen abstraction leading to Ge_2H_5 and H_2, whereas the substitution reaction with frontside attack becomes the dominant channel at higher temperatures. The substitution reaction with backside attack is a minor channel over the whole studied temperature range.

Digermane Ge_2H_6 is a common precursor used in chemical vapor deposition (CVD)[1–4] to produce semiconductor devices. The reaction with atomic hydrogen, the simplest free-radical species, is of particular interest: kinetics parameters for the H-atom reaction are desirable not only to provide an uncomplicated probe of chemical reactivity but also to throw light on the mechanism of CVD processes. However, despite its importance, studies of the kinetics have been very limited. Only one experimental study is on record. Austin and Lampe[5] measured relative rate constant in competitive experiments at 305 K in a static system, in which H atoms were produced by Hg-sensitized photolysis of H_2, and the rate of loss of Ge_2H_6 was compared with that of C_2H_4 by means of time-of-flight mass spectrometry. To the best of our knowledge, little theoretical attention has been paid to this reaction.

In this paper, we present a theoretical study on the reaction of atomic H with Ge_2H_6. First we have examined the reaction mechanism at high levels of *ab initio* molecular orbital theory. In a second step, we have carried out the kinetics calculations for this reaction. The important features of this study are the following: (1) *ab initio* calculations have been performed for stationary points and for some additional points along the minimum energy paths (MEP) to obtain potential energy information; (2) the nature of the kinetics has been studied over the temperature range from 200 to 3000 K using interpolated canonical variational transition state theory (CVT)[6–8] and the centrifugal-dominant, small-curvature tunneling approximation (SCT),[9] including information at the reactants, products, transition states, and additional points along the minimum energy path; (3) the calculated rate constants are compared with the limited experimental data and (4) the branching ratios are discussed.

Computational methods

Ab initio calculations have been carried out using Gaussian 94 programs.[10] In the entire paper, UMP2 and UQCISD(T) denote the unrestricted versions of MP2 and QCISD(T), respectively. The geometries of the reactant, transition states and products have been optimized at the MP2/6-311G(d) level. The vibrational frequencies have been calculated at the same level in order to determine the nature of the stationary points, the zero-point energy (ZPE), and the thermal contributions to the free energy of activation. Each transition state was verified to connect the designated reactants and products by performing an intrinsic reaction coordinate (IRC) analysis. At the MP2/6-311G(d) level, the minimum energy paths (MEP) were constructed for both abstraction and substitution channels independently, starting from the respective saddle point geometries and going downhill to both the asymptotic reactant and product channels with a gradient step size of 0.02 $amu^{1/2}$ bohr. Along these MEPs the reaction coordinate, s, is defined as the signed distance from the saddle point, with $s > 0$ referring to the product side. In addition, for 30 non-stationary points near the transition state along the MEP, 15 points on the reactant side and 15 points on the product side, we computed the gradients and Hessians at the MP2/6-311G(d) level, avoiding all the time undesirable reorientations of molecular geometries.

Although the geometrical parameters and the frequencies of various species can be determined satisfactorily at the MP2/6-311G(d) level, the energies obtained at this level may not be accurate enough for the subsequent kinetics calculation. Therefore, a higher level, QCISD(T), and a more flexible basis set, 6-311+G(3df,2p), were employed to calculate the energies of various species.

The initial information obtained from our *ab initio* calculations allowed us to calculate the variational rate constants including the tunneling effect. The canonical variational theory (CVT)[6–8] rate constant for temperature T is given by:

$$k^{\mathrm{CVT}}(T) = \min_{s} k^{\mathrm{GT}}(T,s) \quad (1)$$

with

$$k^{\mathrm{GT}}(T,s) = \frac{\sigma k_{\mathrm{B}} T}{h} \frac{Q^{\mathrm{GT}}(T,s)}{\Phi^{\mathrm{R}}(T)} e^{-V_{\mathrm{MEP}}(s)/k_{\mathrm{B}}T} \quad (2)$$

where $k^{\mathrm{GT}}(T,s)$ is the generalized transition state theory rate constant at the dividing surface s, σ is the symmetry factor accounting for the possibility of more than one symmetry-related reaction path, k_{B} is Boltzmann's constant, h is Planck's constant, $\Phi^{\mathrm{R}}(T)$ is the reactant partition function per unit volume, excluding symmetry numbers for rotation, and $Q^{\mathrm{GT}}(T,s)$ is the partition function of a generalized transition state at s with a local zero of energy at $V_{\mathrm{MEP}}(s)$ and with all rotational symmetry numbers set to unity. The tunneling contribution has been included by using the centrifugal-dominant small-curvature semiclassical adiabatic ground state (CD-SCSAG) method.[9] All the kinetics calculations have been carried out using the POLYRATE 7.8 program.[11] The interpolated variational transition state theory by mapping (IVTST-M) was chosen.[12] The rotational partition functions were calculated classically and the vibrational modes were treated as quantum-mechanical separable harmonic oscillators.

Results and discussion

The optimized geometries of the reactant, transition states, and products are shown in Fig. 1. The transition state of the abstraction channel is denoted as TS_1, while the transition states of the substitution channels for frontside and backside attack are denoted as TS_{2a} and TS_{2b}. The vibrational frequencies of the reactant, products, and transition states are listed in Tables 1 and 2. The potential barrier ΔE^{TS} and the reaction enthalpy ΔH calculated are summarized in Table 3. Fig. 2 shows the classical potential energy (V_{MEP}) and vibrationally adiabatic potential energy ($V_{\mathrm{a}}^{\mathrm{G}}$) curves as functions of distance along the reaction coordinate s at the QCISD(T)/6-311 + G(3df,2p)//MP2/6-311G(d) level for each channel. Change curves of generalized normal-mode vibrational

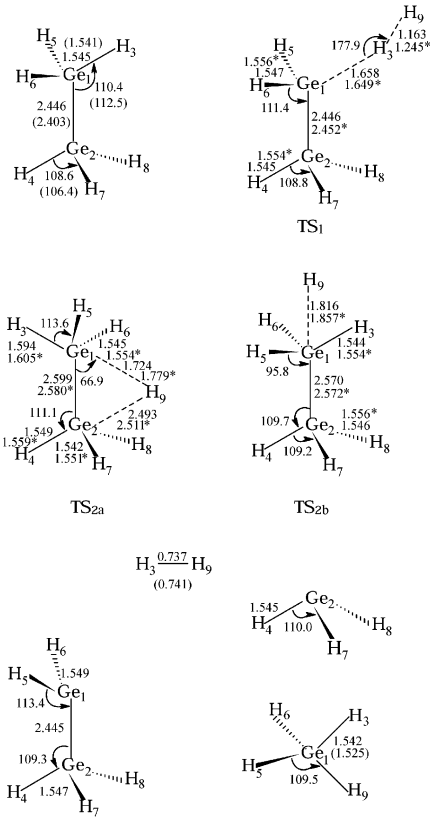

Fig. 1 MP2/6-311G(d) optimized geometries for the stationary points. Distances are in angstroms and angles are in degrees. The values in parentheses are experimental data.[13–15] The values marked with asterisks are the calculated results at the QCISD/6-311G(d) level.

Table 1 Vibrational frequencies (in cm^{-1}) for the reactant and products involved in the reaction of H with Ge_2H_6 at the MP2/6-311G(d) level. The values in italics are the experimental data[15–17]

Species	Frequencies
Ge_2H_6	2141, 2141, 2138, 2133, 2133, 2131, 889, 889, 884, 884, 843, 764, 567, 567, 361, 360, 267, 116
	2091, 2091, 2077, 2073, 2073, 2068, 880, 880, 879, 879, 832, 756, 562, 562, 370, 370, 268, 146
Ge_2H_5	2145, 2142, 2122, 2119, 2101, 884, 882, 862, 789, 573, 552, 395, 371, 262, 112
GeH_4	2161, 2156, 2156, 2156, 924, 924, 826, 826, 826
	2114, 2114, 2114, 2106, 946, 946, 834, 834, 834
GeH_3	2144, 2143, 2118, 861, 861, 710
H_2	4380
	4404

Table 2 Vibrational frequencies (in cm^{-1}) for the transition states involved in the reaction of H with Ge_2H_6 at the MP2/6-311G(d) level

Species	Frequencies
TS_1	2142, 2139, 2134, 2128, 2119, 1114, 966, 930, 885, 885, 860, 787, 606, 586, 427, 399, 291, 265, 171, 91, 1609i
TS_{2a}	2154, 2146, 2135, 2125, 2110, 1817, 1157, 956, 889, 869, 864, 807, 757, 658, 647, 448, 410, 222, 179, 42,[a] 330i
TS_{2b}	2133, 2133, 2125, 2125, 2118, 2077, 1010, 877, 877, 860, 860, 770, 732, 732, 420, 420, 248, 248, 225, 128, 872i

[a] The lowest frequency vibration of the transition state is considered as an internal rotation.

Table 3 The energy barriers ΔE^{TS} (in kcal mol^{-1}) and the reaction enthalpies ΔH (in kcal mol^{-1}) calculated at the MP2/6-311G(d) optimized geometry for each channel involved in the reaction of H with Ge_2H_6 at various levels.[a] The values in italics are the energy barriers and the reaction enthalpies with the ZPE correction

Levels	$\Delta E^{\mathrm{TS_1}}$	$\Delta E^{\mathrm{TS_{2a}}}$	$\Delta E^{\mathrm{TS_{2b}}}$	ΔH_1	ΔH_2
MP2/6-311G(d)	8.37	15.86	15.38	−17.00	−10.08
	7.97	*17.55*	*16.68*	*−16.20*	*−7.82*
PMP2/6-311G(d)	6.40	13.22	12.31	−17.49	−10.39
	6.00	*14.91*	*13.61*	*−16.69*	*−8.13*
MP2/6-311 + G(3df,2p)	5.22	9.93	11.65	−20.34	−14.64
	4.82	*11.62*	*12.92*	*−19.54*	*−12.38*
PMP2/6-311 + G(3df,2p)	3.24	7.24	8.57	−20.92	−15.03
	2.84	*8.93*	*9.87*	*−20.12*	*−12.77*
QCISD(T)/6-31 + G(3df,2p)	2.17	5.42	7.22	−22.62	−17.36
	1.77	*7.11*	*8.52*	*−21.82*	*−15.10*
QCISD(T)/6-31 + G(3df,2p)[a]	2.41	5.86	7.56	−22.64	−17.33

[a] $\Delta E^{\mathrm{TS_1}}$, $\Delta E^{\mathrm{TS_{2a}}}$, $\Delta E^{\mathrm{TS_{2b}}}$ are the energy barriers of the abstraction channel and the substitution channels with frontside attack and backside attack. ΔH_1 and ΔH_2 are the reaction enthalpies of the abstraction and the substitution channels, respectively. [b] At the QCISD/6-311G(d) optimized-geometry.

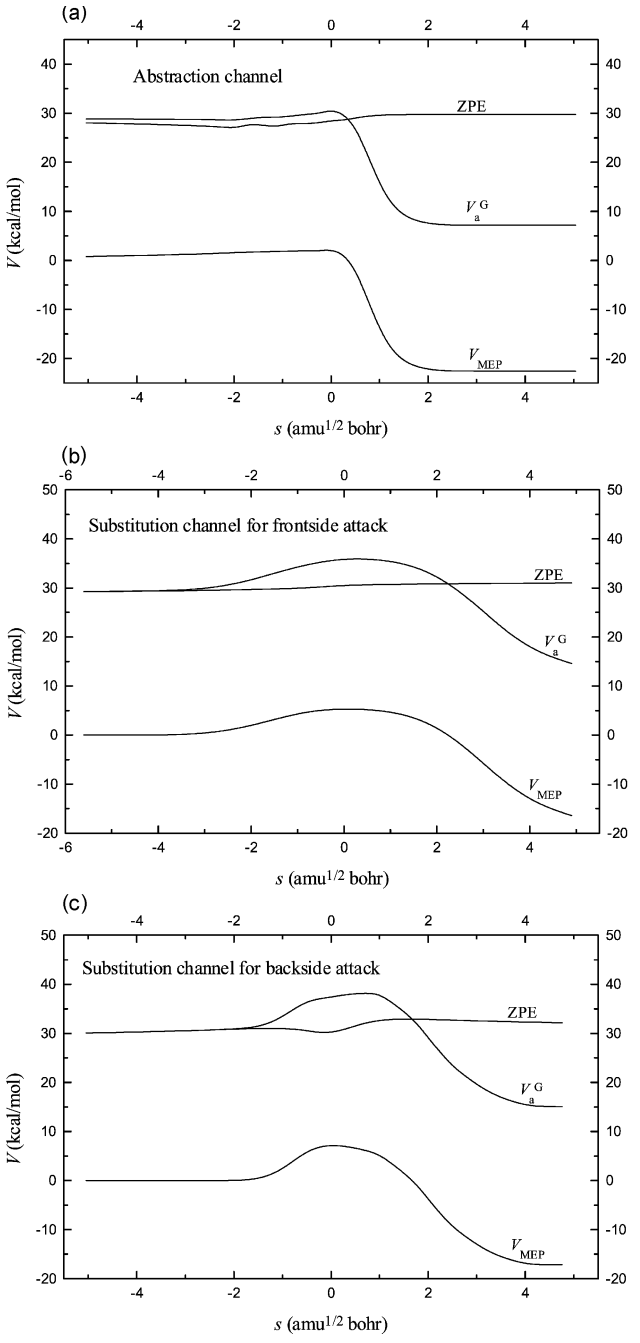

Fig. 2 The classical potential energy (V_{MEP}) and vibrationally adiabatic potential energy (V_a^G) curves as a function of s at the QCISD(T)/6-311+G(3df,2p)//MP2/6-311G(d) level for all the channels.

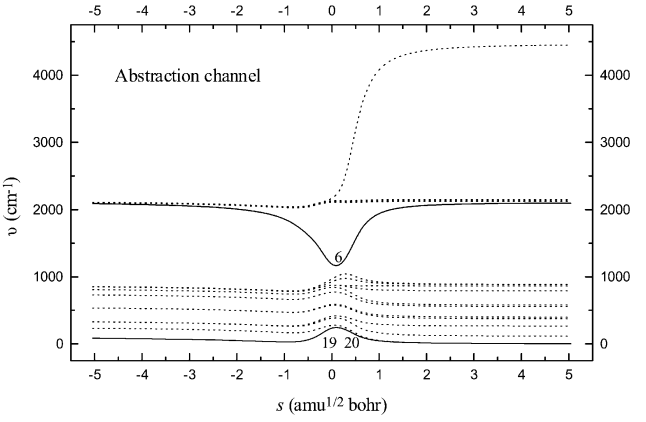

Fig. 3 Changes of the generalized normal-mode vibrational frequencies as a function of s at the MP2/6-311G(d) level for the abstraction channel.

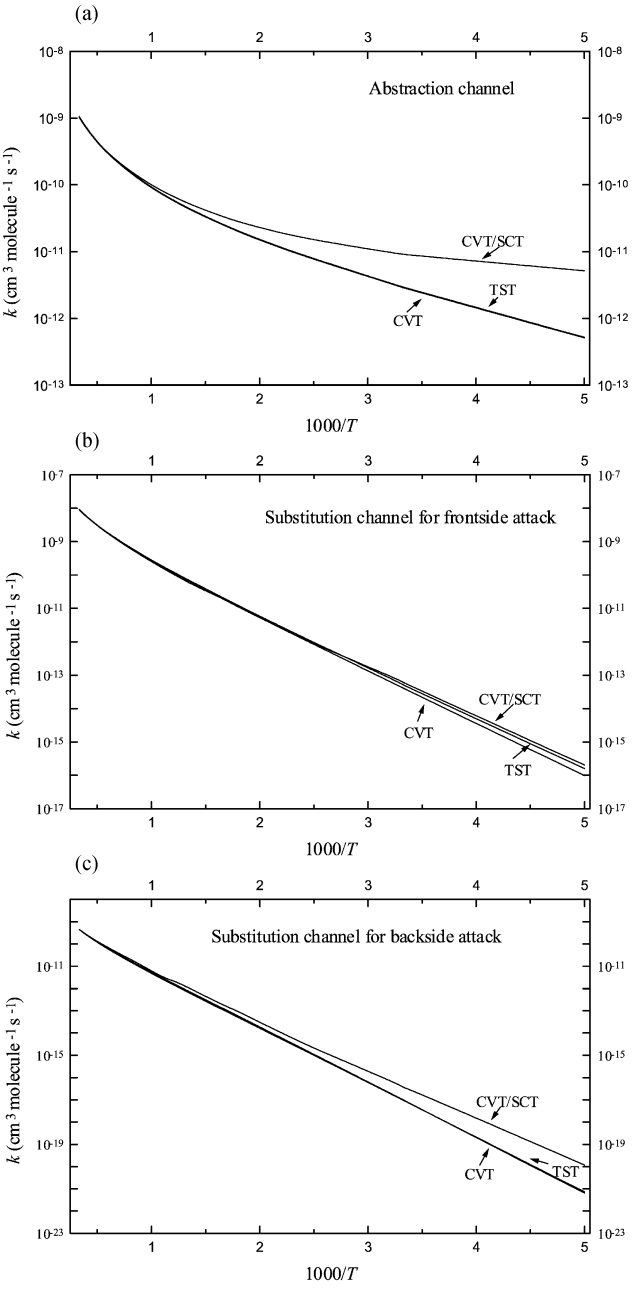

Fig. 4 Rate constants as a function of the reciprocal of the temperature (T)over the range of 200–3000 K for the all the channels.

frequencies with the reaction coordinate s are shown in Fig. 3 for the abstraction channel. The calculated TST, CVT, and CVT/SCT rate constants are presented in Fig. 4 over the temperature range of 200–3000 K for all the channels. The CVT/SCT rate constants and the branching ratios for each channel are summarized in Table 4.

Reaction mechanism

Geometry and frequency. The reactant digermane has two geometries: the staggered and the eclipsed. The energy of the eclipsed is higher than that of the staggered.

To clarify the general reliability of the theoretical calculations, it is useful to compare the predicated chemical properties with experimental data. As shown in Fig. 1, the geometric parameters of Ge_2H_6, GeH_4 and H_2 are in good agreement

Table 4 The CVT/SCT rate constants and the branching ratios for all the channels involved in the reaction of Ge_2H_6 with H over the temperature range of 200–3000 K (in cm^3 $molecule^{-1}$ s^{-1})

T/K	k_1	k_{2a}	k_{2b}	k	k_1/k	k_2/k
200	5.17E-12	2.01E-16	1.18E-20	5.17E-12	1.00	0.00
298	9.00E-12	5.44E-14	3.45E-17	9.05E-12	1.00	0.00
300	9.10E-12	5.97E-14	3.40E-17	9.15E-12	0.99	0.01
305	9.30E-12	7.47E-14	5.20E-17	9.41E-12	0.99	0.01
400	1.50E-11	8.53E-13	2.00E-15	1.58E-11	0.95	0.05
450	1.87E-11	2.36E-12	9.18E-15	2.11E-11	0.89	0.11
500	2.30E-11	5.40E-12	2.97E-14	2.84E-11	0.81	0.19
550	2.77E-11	1.07E-11	8.37E-14	3.85E-11	0.72	0.28
600	3.32E-11	1.90E-11	1.78E-13	5.23E-11	0.63	0.37
700	4.59E-11	4.20E-11	6.59E-13	8.85E-11	0.52	0.48
800	6.12E-11	8.68E-11	1.85E-12	1.50E-10	0.41	0.59
1000	9.95E-11	2.53E-10	6.26E-12	3.58E-10	0.28	0.72
1200	1.48E-10	5.40E-10	1.77E-11	7.06E-10	0.21	0.79
1400	2.07E-10	9.61E-10	3.46E-11	1.20E-9	0.17	0.83
1600	2.77E-10	1.53E-9	5.87E-11	1.86E-9	0.15	0.85
2000	4.47E-10	3.08E-9	1.30E-10	3.66E-9	0.12	0.88
2400	6.56E-10	5.15E-9	2.32E-10	6.04E-9	0.11	0.89
2800	9.01E-10	7.73E-9	3.63E-10	9.00E-9	0.10	0.90
3000	1.04E-9	9.20E-9	4.39E-10	1.07E-8	0.10	0.90

with the available experimental values. In order to further check the reliability of the MP2-computed geometry, we performed the QCISD calculation with the 6-311G(d) basis set (computationally more expensive) for the transition states. The optimized geometrical parameters are also shown in Fig. 1. Compared with the results calculated at the MP2/6-311G(d) level, it can be seen that extension of the calculation level to QCISD does not cause observable change. As can be seen from Table 2, the vibrational frequencies of Ge_2H_6, GeH_4 and H_2 agree well with the experimentally observed fundamentals, and the maximum relative error is less than 3%. This good agreement gives us confidence that the MP2/6-311G(d) theory level is adequate to optimize the geometries and calculate the frequencies.

As mentioned above, two primary processes have been identified in the reaction of atomic H with Ge_2H_6: abstraction

$$H_3Ge–GeH_3 + H \rightarrow H_3Ge–GeH_2 + H_2$$

and substitution

$$H_3Ge–GeH_3 + H \rightarrow H_3Ge + GeH_4$$

The transition state of the abstraction channel is denoted as TS_1; its geometrical structure is shown in Fig. 1. The incoming H atom attacks one H of Ge_2H_6 with a slightly bent orientation angle of 177.9°. At the MP2/6-311G(d) level, the forming H_3–H_9 bond of 1.163 Å is 57.8% longer than the equilibrium value of 0.737 Å in H_2, while the breaking Ge_1–H_3 bond is stretched by 7.3%. The transition state TS_1 is reactant-like. Therefore, the hydrogen abstraction reaction from Ge_2H_6 by H will proceed *via* an early transition state. This rather early character of the transition state TS_1 is in accordance with the low reaction barrier and the high exothermicity of this abstraction reaction, in keeping with Hammond's postulate. The transition state was identified with one negative eigenvalue of the Hessian matrix and, therefore, one imaginary frequency. Since the imaginary frequency governs the width of the classical potential energy barrier along the MEP, it plays an important role in the tunneling calculations, especially when the imaginary frequency is large, and the associated eigenvector has a large component of hydrogenic motion. For the abstraction channel, the imaginary frequency is 1609i, so we expect that the tunneling effect should be important for the calculation of the rate constant. The transition state TS_1 has C_s symmetry.

Since atomic hydrogen has both nucleophilic and electrophilic character, there are two transition state structures for the substitution reaction: (1) a frontside attack on the Ge–Ge bond by the H atom and (2) a backside attack of the GeH_3 group. The transition states for frontside attack and backside attack are denoted as TS_{2a} and TS_{2b}, respectively, and their geometrical parameters are shown in Fig. 1. At the MP2/6-311G(d) level, the structure of the transition state TS_{2a} shows the incoming H atom is more closely associated with Ge_1. This results in a strong five-coordinate environment around Ge_1 while Ge_2 remains primarily four-coordinate. The breaking Ge_1–Ge_2 bond is 0.153 Å longer than the corresponding value in digermane. The forming Ge_1–H_9 bond of 1.724 Å is 11.8% longer than the equilibrium value in GeH_4. The hydrogen (H_3) that is trans to the incoming hydrogen H_9 has a longer bond length (1.594 Å) to Ge_1 than the other two hydrogens (H_5 and H_6). The transition state TS_{2a} has one and only one imaginary frequency. Direct inspection of the transition state low-frequency mode indicates that the mode of the lowest frequency (42 cm^{-1}) is a hindered internal rotation instead of a small-amplitude vibration. This mode was removed from the vibrational partition function for the transition state and the corresponding hindered rotor partition function $Q_{HR}(T)$, calculated by the method devised by Truhlar,[18] was included in the expression for the rate constants. The transition state TS_{2a} has C_s symmetry.

For the substitution reaction with backside attack, the attacking H atom interacts with a germanium center along the Ge–Ge axis, forming a transition state with high symmetry C_{3v}. For the transition state TS_{2b} of the backside attack reaction, the MP2 structure has a strong five-coordinate environment around Ge_1 and a nearly tetrahedral geometry around Ge_2. The geometric parameters for the local environment around Ge_2 have not significantly changed from the corresponding values in digermane. The breaking Ge_1–Ge_2 bond is 0.124 Å longer than the equilibrium value in Ge_2H_6, while the forming Ge_1–H_9 bond is stretched by 17.8%. The transition state TS_{2b} has one and only one imaginary frequency. The value of the imaginary frequency is large, which implies that the quantum tunneling effect may be significant and may play an important role in the calculation of the rate constant.

In order to further confirm that these transition states connect the designated reactants and products, the intrinsic reaction coordinate (IRC) has been calculated at the MP2/6-311G(d) level from the transition state to the reactants and the products. For the abstraction channel, the breaking Ge_1–H_3 bond remains insensitive up to $s = -0.5$ $amu^{1/2}$ bohr and then increases smoothly. Meanwhile, the forming H_3–H_9 bond shortens rapidly from reactants and reaches the equilibrium bond length in H_2 at $s = 0.7$ $amu^{1/2}$ bohr. Other bond lengths are almost unchanged during the reaction process. Therefore, the geometric change mainly takes place in the region from $s = -0.5$ to $s = 0.7$ $amu^{1/2}$ bohr for the abstraction channel. For the substitution channels with frontside attack and backside attack, the change curves of the bond lengths with the reaction coordinate s are very similar. First, while the lengths of the breaking bond Ge_1–Ge_2 and the forming bond Ge_1–H_9 change strongly in the course of the reaction, the other bond lengths do not change. Second, the geometrical changes take place over a wider range, from $s = -3.5$ to $s = 3.0$ $amu^{1/2}$ bohr for frontside attack and from $s = -1.5$ to $s = 2.0$ $amu^{1/2}$ bohr for backside attack.

Energy. Table 3 summarizes uncorrected and zero-point-corrected barrier heights ΔE^{TS} and reaction enthalpies ΔH relative to the reactants at the MP2/6-311G(d)-optimized geometries for each channel involved in the reaction of H with Ge_2H_6.

With respect to the potential barrier, the values obtained at the MP2 and QCISD(T) levels show great discrepancies for the

same channel. The potential barriers obtained from the MP2 energies are found to be more than 1.5 kcal mol^{-1} higher than those obtained from the corresponding PMP2 energies (annihilated spin contamination) for all the channels. The effect of the basis set on the potential barrier can be observed from our MP2 result with two different basis sets, namely 6-311G(d) and 6-311 + G(3df,2p). The barrier heights without ZPE correction decrease by 3.15, 5.93 and 3.73 kcal mol^{-1} with the increase in basis sets at the MP2 level for the abstraction channel and substitution channels with frontside attack and backside attack, respectively. As we raise the calculation levels [MP2 → QCISD(T)], the barrier height is lowered drastically. We take the QCISD(T)/6-311 + G(3df,2p) level as the most reliable level.

Because of the absence of experimental standard heats of formation for the present reaction system, it is difficult to make a conclusive comparison on the reaction enthalpy. Spin contamination in the product radicals is much less compared to that observed in TSs: the values of $\langle S^2 \rangle$ for Ge_2H_5 and GeH_3 do not exceed 0.757, while the values of $\langle S^2 \rangle$ are in the range of 0.779–0.804 for the transition states of the abstraction and substitution channels. Thus, the differences between the MP2 and PMP2 values for the reaction enthalpy are much less significant than those for the potential barrier.

At the QCISD/6-311G(d)-optimized geometry, we calculated the potential barriers and the reaction enthalpies at the QCISD(T)/6-311 + G(3df,2p) level. As seen from Table 3, the potential barriers at the QCISD(T)/6-311 + G(3df,2p)//MP2/6-311G(d) level agree with the potential barriers at the QCISD(T)/6-311 + G(3df,2p)//QCISD/6-311G(d) level within 0.42 kcal mol^{-1} for all channels. The reaction enthalpies are almost equal at the QCISD(T)/6-311 + G(3df,2p)//MP2/6-311G(d) and QCISD(T)/6-311 + G(3df,2p)//QCISD/6-311G(d) levels. Although the QCISD/6-311G(d) level can result in better geometrical parameters, it needs greater computing condition and it is very time consuming to optimize the geometries and calculate the frequencies for the reaction of Ge_2H_6 with atomic H. Therefore, in this paper, we chose the potential barriers and the reaction enthalpies calculated at the QCISD(T)/6-311 + G(3df,2p)//MP2/6-311G(d) level for the following kinetics calculations. At the QCISD(T)/6-311 + G(3df,2p)//MP2/6-311G(d) level, the abstraction reaction has the smallest potential barrier of 2.17 kcal mol^{-1}. The barrier height without ZPE correction for frontside attack is 3.10 kcal mol^{-1} lower than that for backside attack. This means that the substitution reaction will occur mainly by frontside attack.

Kinetics calculations

Reaction path properties. The minimum energy path (MEP) was calculated at the MP2/6-311G(d) level by the IRC definition, and the energies of the MEP were refined by the QCISD(T)//MP2 method. For all channels the maximum position of the classical potential energy curve V_{MEP} at the QCISD(T)//MP2 level corresponds to the saddle point structure at the MP2/6-311G(d) level. Therefore, shifting of the maximum position of the V_{MEP} curve caused by the computational technique is avoided.[19] The changes of the classical potential energy V_{MEP} and the ground-state vibrational adiabatic potential energy V_a^G with the reaction coordinate s are shown in Fig. 2(a–c) for all the channels. The classical potential energy V_{MEP} curve has a narrow shape for the abstraction channel. Therefore, it is expected that the tunneling effect will play an important role in the calculation of the rate constants. Meanwhile, the V_{MEP} curve has the widest shape for the substitution reaction *via* frontside attack, so the tunneling effect may be unimportant here. The V_{MEP} and V_a^G curves are similar in shape, and their maximum positions are almost the same at the QCISD(T)//MP2 level for all the channels. This means that the variational effect will be small for both abstraction and substitution channels. The zero-point energy, ZPE, which is the difference of V_a^G and V_{MEP}, is also shown in Fig. 3. The zero-point energy curve is almost unchanged as s varies. In order to analyze this behavior in greater detail, we show the variation of the generalized normal mode vibrational frequencies in Fig. 3 for the abstraction channel.

In the negative limit of s, the frequencies are associated with the reactants, while in the positive limit of s, the frequencies are associated with the products. For the abstraction channel, the frequency of the vibrational mode 6 (reactive mode), which connects the Ge–H stretching vibration in Ge_2H_6 with the H–H stretching vibration of H_2, drops dramatically from $s = -1.0$ to $s = 1.0$ amu$^{1/2}$ bohr. This behavior is typical of hydrogen transfer reactions.[20–22] If changes in other frequencies were small, this drop could cause a considerable fall in the zero-point energy near the transition state. The two lowest harmonic vibrational frequencies (modes 19 and 20, transitional modes) along the reaction path correspond to the transformation of free rotations or free translations of the reactants into real vibrational motions in the global system. Their frequencies tend asymptotically to zero at the reactant and product limits, and they reach their maximum in the saddle point zone. Therefore, in the saddle point region, the behavior of these transitional modes compensates the fall in the zero-point energy caused by the reactive mode. As a result, the zero-point energy curve shows little variation with s. For the substitution channels with frontside and backside attack, the frequency of the mode related to the breaking/forming bonds drops (reactive mode) dramatically near the saddle point. However, this drop is compensated by the transitional modes. Therefore, the zero-point energy curve for the substitution channels is also almost unchanged as s varies.

Rate constants. The canonical variational transition state theory (CVT) with a small-curvature tunneling correction (SCT), which has been successfully performed for several analogous reactions,[23–25] is an efficient method to calculate rate constants. In this paper, we used this method to calculate the rate constants for all the channels involved in the reaction of H atom with Ge_2H_6 over a wide temperature range, from 200 to 3000 K. The calculated CVT/SCT rate constants are shown in Fig. 4(a–c). For the purpose of comparison, the conventional transition state theory (TST) rate constants and the variational transition state theory (CVT) rate constants without the tunneling correction are also shown in Fig. 4(a–c). Several important features of the calculated rate constants are the following:

(1) For both abstraction and substitution channels, the TST and the CVT rate constants are almost the same over the entire studied temperature range, which enables us to conclude that the variational effect is small for the calculation of the rate constant.

(2) For the abstraction channel, in the temperature range of 200–550 K, the CVT rate constants are much smaller than those from the CVT/SCT calculation. For example, at 298 K, the CVT rate constant is 2.81×10^{-12} cm^3 molecule^{-1} s^{-1}, while the CVT/SCT rate constant is 8.99×10^{-12} cm^3 molecule^{-1} s^{-1}. The latter is 3.2 times larger than the former. The difference between the CVT and the CVT/SCT rate constants decreases with increase in temperature. At temperatures above 1000 K, the CVT/SCT rate constants asymptotically approach the CVT rate constants, which means that only in the lower temperature range does the small-curvature tunneling correction play an important role in the calculation of the rate constant. For the substitution channel *via* frontside attack, the CVT/SCT rate constants are very close to the CVT rate constants over the whole studied temperature range, which means that the small-curvature tunneling correction is unimportant for this channel. For the substitution channel

via backside attack, in the temperature range of 200–1000 K, the CVT rate constants are smaller than the CVT/SCT ones. When the temperature is higher than 1000 K, the CVT and CVT/SCT rate constants are almost the same. This means the tunneling effect can be neglected in the higher temperature range for the substitution channel with backside attack.

(3) At 305 K, the total CVT/SCT rate constant, which is the sum of the CVT/SCT rate constants for all the channels, is 9.40×10^{-12} cm^3 molecule^{-1} s^{-1}, which is in good agreement with the experimental value of 1.6×10^{-11} cm^3 molecule^{-1} s^{-1}. Both the TST and the CVT methods without the tunneling effect correction underestimate the rate constants. Therefore, the CVT/SCT rate constants are taken as the accurate ones for each channel.

(4) In order to provide clear information about the branching ratio, we have listed the CVT/SCT rate constants and the branching ratios of each channel in Table 4. The CVT/SCT rate constants of the abstraction channel are noted as k_1, while the rate constants of the substitution reaction with frontside and backside attack are noted as k_{2a} and k_{2b}. The total rate constants of the substitution reaction are noted as k_2, where $k_2 = k_{2a} + k_{2b}$. The overall rate constants are noted as k, with $k = k_1 + k_2$. The branching ratios of the abstraction reaction and the substitution reaction are noted as k_1/k and k_2/k.

As seen from Table 4, hydrogen abstraction is the fastest reaction channel in the temperature range of 200–700 K. However, as the temperature increases, the substitution reaction *via* frontside attack becomes a competitive reaction channel. When the temperature is higher than 1000 K, the substitution reaction with frontside attack becomes the dominant channel. Due to its having the highest barrier height, the contribution of the substitution reaction with backside attack is minor over the whole studied temperature range. In the lower temperature range, the rate constant k_{2b} is so small that it can be neglected, namely $k_2 = k_{2a} + k_{2b} \approx k_{2a}$. For example, at 1000 K the substitution reaction with frontside attack is about 40 times faster than the substitution reaction with backside attack. When $T \geq 2000$ K, the rate constant k_{2b} is not longer negligible and will make some contribution to the branching ratioand to the overall rate constants. For example, at $T = 2400$ K, $k_{2b}/k = 0.4$.

Conclusions

In this paper, we have studied the reaction of H with Ge_2H_6 using *ab initio* electronic structure theory and canonical variational transition state theory (CVT) with small-curvature tunneling (SCT). The reaction mechanism and rate constants were reported over the temperature range of 200–3000 K. Several major conclusions can be drawn from this calculation. (1) At the lower temperatures, hydrogen abstraction is the major channel. With increasing temperature, the substitution reaction with frontside attack becomes the dominant channel. Due to its having the highest barrier height, the substitution reaction with backside attack is a minor channel. (2) The variational effect is small for both abstraction and substitution channels. (3) In the lower temperature range, the small-curvature tunneling contribution plays an important role for the abstraction channel and the substitution channel with backside attack. (4) At 305 K, the CVT/SCT overall rate constant is in good agreement with the experimental value. Both the TST method and the CVT method without tunneling underestimate the rate constants.

Acknowledgements

The authors thank Professor Donald G. Truhlar for providing the POLYRATE 7.8 program. This work is supported by the Research Fund for the Doctoral Program of Higher Education of China.

References

1 H. Kim, N. Taylor, T. R. Bramblett and J. E. Greene, *J. Appl. Phys.*, 1998, **84**, 6372.
2 C. Li, S. John and S. Banerjee, *J. Electron. Mater.*, 1995, **24**, 875.
3 D.-S. Lin, T. Miller and T.-C. Chiang, *J. Vac. Sci. Technol., A*, 1997, **15**, 919.
4 A. F. Aguilera, K. H. Pannell and J. Craig, Jr., *Congr. Iberoam. Quim. Inorg. 6th*, 1997, p. 307.
5 E. R. Austin and F. W. Lampe, *J. Phys. Chem.*, 1977, **81**, 1134.
6 K. K. Baldridge, M. S. Gordon, R. Steckler and D. G. Truhlar, *J. Phys. Chem.*, 1989, **93**, 5107.
7 A. Gonzalez-Lafont, T. N. Truong and D. G. Truhlar, *J. Chem. Phys*, 1991, **95**, 8875.
8 B. C. Garrett and D. G. Truhlar, *J. Phys. Chem.*, 1979, **83**, 1052.
9 Y.-P. Liu, G. C. Lynch, T. N. Truong, D.-H. Lu, D. G. Truhlar and B. C. Garrett, *J. Am. Chem. Soc.*, 1993, **115**, 2408..
10 M. J. Frisch, G. W. Trucks, H. B. Schlegel, P. W. M. Gill, B. G. Johnson, M. A. Robb, J. R. Cheeseman, T. A. Keith, G. A. Petersson, J. A. Montgomery, K. Raghavachari, M. A. Allaham, V. G. Zakrzewski, J. V. Ortiz, J. B. Foresman, J. Cioslowski, B. B. Stefanov, A. Nanayakkara, M. Challacombe, C. Y. Peng, P. Y. Ayala, W. Chen, M. W. Wong, J. Andres, E. S. Replogle, R. Gomperts, R. L. Martin, D. J. Fox, J. S. Binkley, D. J. Defrees, J. Baker, J. P. Stewart, M. Head-Gordon, C. Gonzales, J. A. Pople, GAUSSIAN94, Revision E.1, Gaussian, Pittsburgh, PA, 1995.
11 R. Steckler, Y. Y. Chuang, P. L. Fast, J. C. Corchade, E. L. Coitino, W. P. Hu, G. C. Lynch, K. Nguyen, C. F. Jackells, M. Z. Gu, I. Rossi, S. Clayton, V. Melissas, B. C. Garrett, A. D. Isaacson and D. G. Truhlar, POLYRATE,version 7.8, University of Minnesota, Minneapolis, 1997.
12 J. C. Corchado, E. L. Coitino, Y.-Y. Chuang, P. L. Fast and D. G. Truhlar, *J. Phys. Chem, A*, 1998, **102**, 2424.
13 H. Oberhammer, T. Lobreyer and W. Sundermeyer, *J. Mol. Struct.*, 1994, **323**, 125.
14 J. H. Collomon, E. Hirota, K. Kuchitsu, W. J. Lafferty, A. G. Maki and C. S. Pote, *Structure Data of Free Polyatomic Molecules*, Springer-Verlag, Berlin, 1976, vol. 7.
15 *JANAF Thermochemical Tables*, ed. M. W. Chase, Jr., C. A. Davies, J. R. Downey, D. J. Frurip, R. A. McDonald and A. N. Syverud, National Bureau of Standards, Washington, D. C., 3rd edn., 1985, vol. 14.
16 J. E. Griffiths and G. E. Walrafen, *J. Chem. Phys.*, 1964, **40**, 321.
17 T. Shimanouchi, *Tables of Molecular Vibrational Frequencies*, National Standard Reference Data Series, NBS–US GPO, Washington, D. C., 1972, vol. 39.
18 D. G. Truhlar, *J. Comput. Chem.*, 1991, **12**, 266.
19 J. Espinosa-Garcia and J. C. Corchado, *J. Phys. Chem.*, 1995, **99**, 8613.
20 D. G. Truhlar and A. D. Isaacson, *J. Chem. Phys.*, 1982, **77**, 3516.
21 J. Espinosa-Garcia and J. C. Corchado, *J. Phys. Chem.*, 1996, **100**, 16 561.
22 J. C. Corchado and J. Espinosa-Garcia, *J. Chem. Phys.*, 1997, **106**, 4013.
23 Q.-Z. Zhang, S.-K. Wang and Y.-S. Gu, *J. Phys. Chem. A*, 2002, **106**, 3796.
24 Q.-Z. Zhang, D.-J. Zhang, S.-K. Wang and Y.-S. Gu, *J. Phys. Chem. A*, 2002, **106**, 122.
25 Y. X. Yu, S. M. Li, Z. F. Xu, Z. S. Li and C. C. Sun, *Chem. Phys. Lett.*, 1999, **302**, 281.